Can a Single-Pulse Standing Wave Induce Chaos in Atomic Motion?

J. C. Robinson, C. F. Bharucha, K. W. Madison, F. L. Moore,* Bala Sundaram, S. R. Wilkinson, and M. G. Raizen

Department of Physics, The University of Texas at Austin, Austin, Texas 78712-1081
(Received 31 October 1995)

We measure momentum transferred from a single pulse of a standing wave of light to a sample of ultracold sodium atoms, and observe a sharp increase in the momentum transfer when the pulse duration exceeds a critical value τ_{cr}. A classical analysis of nonlinear resonances shows that resonance overlap occurs at τ_{cr}, and there is a transition to global classical chaos. These results are a direct experimental test of the "resonance overlap criteria" and illustrate that even the turning on and off of a simple spatially periodic interaction can lead to surprising and novel results.

PACS numbers: 05.45.+b, 32.80.Pj, 42.50.Vk

Time-dependent Hamiltonian dynamics exhibit a wide range of novel effects in both classical and quantum domains [1,2]. Possibly the simplest time-dependent potential is the turning on and off of an interaction, though even here our intuition is clear only for the two extreme cases of fast passage and adiabatic interactions. Since the majority of cases fall between these two limits, it is important to develop a clear understanding and simple physical pictures at intermediate time scales. We show that when the interaction is nonlinear, the mere act of turning on and off a potential in this intermediate regime can lead to classical chaos. Further, we provide a clean experimental demonstration of the *classical mechanism of resonance overlap* [3–5] which leads to classically diffusive growth.

This general problem is posed in the context of atom optics with ultracold atoms. The nonlinear interaction is a single pulse of a one-dimensional standing wave of light. This type of time-dependent interaction is ubiquitous and occurs, for example, whenever an atomic beam passes through a standing wave of light.

The starting point for this discussion is the model of a two level atom (transition frequency ω_0) interacting with a standing wave of near-resonant light (frequency ω_L) which is turned on and off with a time-dependent function $f(t)$. For sufficiently large detuning $\delta_L = \omega_0 - \omega_L$ (relative to the natural linewidth), the excited state amplitude can be adiabatically eliminated [6], leading to a Hamiltonian for the ground state $H = p^2/2M - (\hbar\Omega_{eff}/8)f(t)\cos 2k_L x$. k_L is the wave number, and $\Omega_{eff} = \Omega_0^2/\delta_L$ is the effective Rabi frequency. The resonant Rabi frequency Ω_0 is proportional to the square root of the standing wave intensity [7]. We consider here the case $f(t) = \sin^2 \omega_m t/2$, where ω_m is a radio frequency. In the experiment, only a single pulse of duration $T_s = 2\pi/\omega_m$ is used.

The experimental study of this time-dependent interaction consists of three important components: initial conditions, interaction potential, and measurement of atomic momentum, which occur as a computer-controlled sequence of steps. The sequence is repeated for a range of different interaction pulse durations. The initial conditions consist of ultracold sodium atoms trapped and laser cooled in a standard $\sigma^+ - \sigma^-$ magneto-optic cell trap (MOT) [8]. A single-mode dye laser is intensity stabilized to approximately 1% and servo locked 20 MHz to the red of the $(3S_{1/2}, F = 2) \rightarrow (3P_{3/2}, F = 3)$ transition at 589 nm. Optical pumping to the $F = 1$ ground state is prevented by 15% sidebands at 1.712 GHz. Approximately 10^5 atoms are trapped in a Gaussian distribution of position ($\sigma_x = 0.12$ mm) and momentum (of width σ_p, centered at $p = 0$). This sample is sufficiently dilute that atom-atom interactions are negligible. The experiments therefore probe single-atom phenomena although the measurements are done on an ensemble. After the cooling and trapping stage, the MOT laser beams and gradient coils are turned off. The sidebands are turned off 50 μs prior to the turn off of the MOT beams in order to pump the atoms into the $F = 1$ ground state.

The interaction potential is provided by a second stabilized single-mode dye laser that is retroreflected from a mirror to form a standing wave at the atoms. To ensure a uniform light field the beam is first spatially filtered, and is then focused to a waist which is large (1.2 mm) compared to the atomic sample. A fast acousto-optic modulator (25 ns rise time) controls the single $\sin^2(\pi t/T_s)$ pulse amplitude, where T_s ranges from 100 ns to 5 μs. The first-order diffraction efficiency of an acousto-optic modulator is proportional to $\sin^2(\pi V/2V_{sat})$, where V is the applied voltage, and V_{sat} the saturation voltage. Therefore a linear ramp up and down in V produces the desired line shape. A fast photodiode detects the amplitude as a function of time, which is then digitized and stored. The photodiode output is also measured on an electronic spectrum analyzer to determine spectral purity. The spectrum consists of the fundamental at a frequency of $1/T_s$, and the second harmonic is 20 dB lower. The effect of the second harmonic on the analysis of nonlinear resonances is small and is within our experimental uncertainty. Harmonics higher than the second are negligible.

After the interaction pulse the atoms expand freely for 5 ms, after which the $\sigma^+ - \sigma^-$ beams are turned back on, this time without the magnetic field gradient, forming optical molasses [8]. The motion of the atoms in the

molasses is overdamped and is effectively "frozen" for short times during which the fluorescence is recorded on a charge-coupled device. The resulting 2D image can be integrated to give the 1D distribution along the interaction potential axis. The final spatial distribution, along with the initial spatial distribution and the free-expansion time, enable the determination of the momentum distribution of the atoms.

The measured momentum distributions as a function of pulse duration T_s are shown in Fig. 1. For short interaction times, the final distribution is nearly identical to the initial one ($T_s = 0$) indicating the fast passage limit. With increasing pulse duration the line shape broadens, and undergoes a transition to a flat, broad line shape. For a pulse duration of 1 μs the line shape becomes exponential which is a signature of dynamical localization within a bounded region of momentum, though this is not the focus of this Letter. For even longer times the distribution becomes narrow and asymptotically approaches the initial line shape which is to be expected in the adiabatic limit.

At first sight the dependence of momentum spread on pulse duration appears counterintuitive, and clearly points to new physics that is occurring at intermediate time scales between the limits of fast passage and adiabatic interactions. As we will show below, this behavior is strongly correlated with changes in the classical dynamics. To analyze our problem, we expand the Hamiltonian

$$H = p^2/2M - (\hbar\Omega_{\text{eff}}/8)\sin^2(\omega_m t/2)\cos 2k_L x, \quad (1)$$

and obtain

$$H = p^2/2M - (\hbar\Omega_{\text{eff}}/16)$$
$$\times \{\cos 2k_L x - [\cos 2k_L(x - v_m t)$$
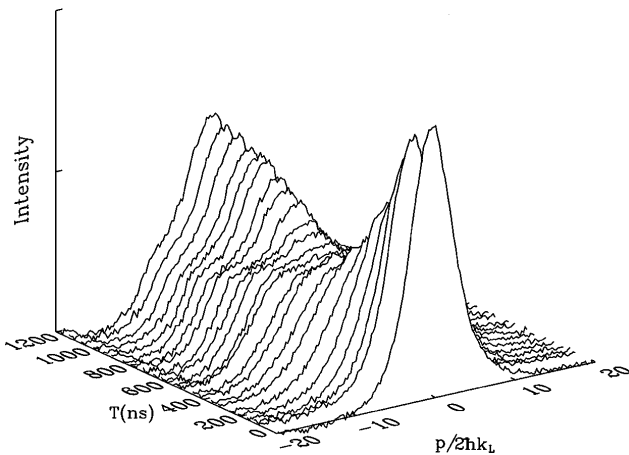$$+ \cos 2k_L(x + v_m t)]/2\}, \quad (2)$$

FIG. 1. Experimentally measured momentum line shapes as a function of pulse duration. The curve at time zero corresponds to the initial condition. $\Omega_{\text{eff}}/2\pi = 50.7$ MHz (rms) with a 10% uncertainty. The initial momentum distribution has a width of 2.9 ± 0.2 in $2\hbar k_L$ units.

where $v_m = \omega_m/2k_L$. The effective interaction is that of a stationary wave with two counterpropagating waves moving at $\pm v_m$.

It is convenient to switch to scaled variables $\tau = \omega_m t$, $\phi = 2k_L x$, $\rho = (2k_L/M\omega_m)p$, and $\mathcal{H} = (4k_L^2/M\omega_m^2)H$ in terms of which

$$\mathcal{H} = \rho^2/2 - k\{\cos\phi - [\cos(\phi + \tau) + \cos(\phi - \tau)]/2\}, \quad (3)$$

where $k = \omega_r\Omega_{\text{eff}}/2\omega_m^2$ and $\omega_r = \hbar k_L^2/2M$ is the recoil frequency ($\omega_r/2\pi = 25$ kHz for sodium). Note that in our system of scaled units, the commutator $[\phi, \rho] = i\bar{k}$, where $\bar{k} = 8\omega_r/\omega_m$. There are three resonances which (from the stationary phase condition) are centered at $\rho/\bar{k}(= p/2\hbar k_L) = 0, \pm\omega_m/8\omega_r$ with widths $\Delta\rho_0/\bar{k} \approx 4\sqrt{k}/\bar{k} = \sqrt{\Omega_{\text{eff}}/8\omega_r}$ and $\Delta\rho_\pm/\bar{k} \approx 2\sqrt{2k}/\bar{k} = \sqrt{\Omega_{\text{eff}}/16\omega_r}$, respectively. When the condition $(\Delta\rho_0 + \Delta\rho_+)/2 > 2/3$ is met [3,4], neighboring resonances overlap and the particle can now classically diffuse in momentum over a bounded region demarcated by confining Kolmogorov-Arnold-Moser surfaces. Operationally, this condition is reached either by increasing the pulse duration for fixed laser intensity, as in our experiments, or by increasing the laser intensity for fixed pulse duration. Substituting for the widths provides an estimate of the time scale τ_{cr}

$$T_s > \tau_{\text{cr}} = \frac{2\sqrt{2}}{3(2 + \sqrt{2})}\frac{2\pi}{\sqrt{\omega_r\Omega_{\text{eff}}}}, \quad (4)$$

beyond which the resonances overlap. On recognizing $\tau_{\text{HO}} = 2\pi/\sqrt{\omega_r\Omega_{\text{eff}}}$ to be the period of the small oscillation limit to the pendulum (harmonic oscillator), the threshold for overlap is given by $T_s > 0.28\tau_{\text{HO}}$.

The three rows of panels in Fig. 2 display the classical phase portraits (top), final momentum distributions calculated from the classical dynamics (middle), and the experimental results together with a quantum simulation (bottom). Each column corresponds to a different single pulse duration. In both the classical and quantum calculations, the initial momentum spread is taken from the temperature measurements in the experiment. The quantum calculation is a space-time integration of the Schrödinger equation starting from a squeezed wave-packet initial condition (see the second paper in Ref. [7] for details).

At these parameter values, resonance overlap is predicted to occur around $\tau_{\text{cr}} = 245$ ns. As illustrated in the first column of panels, for durations less than this value the classical phase space consists of three isolated resonances and the initial distribution remains trapped within the central island. Some "heating" of the initial condition can occur as the distribution spreads within this island. On crossing the threshold for overlap, a chaotic band appears over which the classical particle can diffuse. Quantum effects usually suppress this behavior and lead to dynamical localization [6,7] which results in an exponential line
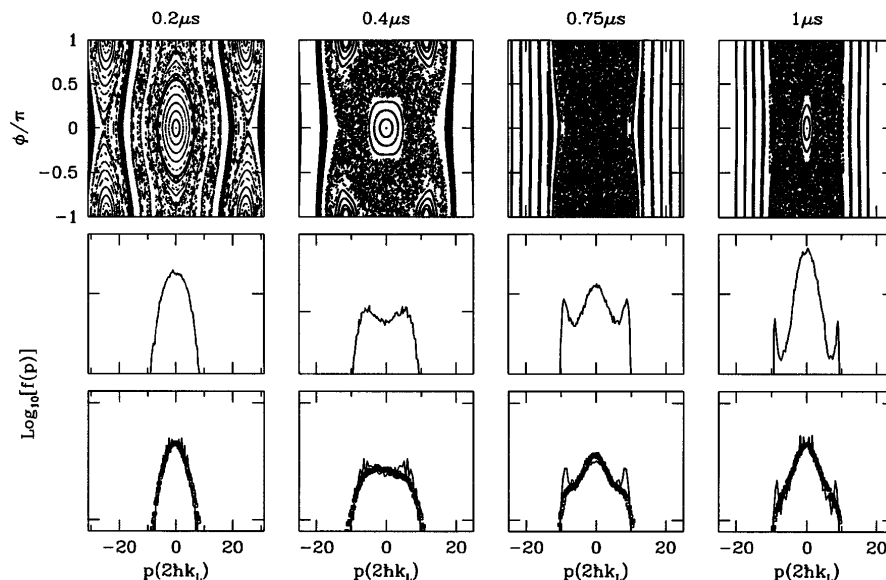
FIG. 2. Classical phase portraits (upper panel), classical momentum distributions (middle panel), and experimentally measured momentum distributions with quantum theory (bottom panel, theory marked by thin lines) for $T_s = 0.2, 0.4, 0.75$, and 1.0 μs. The vertical scales for the distributions are logarithmic and are marked in decades. Other parameters are the same as in Fig. 1.

shape for a pulse duration of $T_s = 1$ μs in Fig. 2. However, for interaction times short compared to the quantum break time [2,9], classical and quantum simulations agree, even in the presence of chaos, as evident in the second and third columns. Both simulations display peaks near the momentum boundaries which show up as less pronounced shoulders in the experimental distributions. This regime of short interaction times in the presence of nearby momentum boundaries is particularly sensitive to variations in $\Omega_{\rm eff}$ present in the experiment. The effect of this variation is similar to having a range of interaction times. We have verified that time averaging resolves the discrepancy between the simulations and the experiment though this is not relevant to the focus of this Letter. It should be noted that for parameters where the adiabatic time scale is comparable to the break time the regime of quantum suppression is not clearly demarcated. As discussed later, the results shown in Fig. 3 illustrate this feature.

To experimentally determine the classical threshold $\tau_{\rm cr}$ for overlap, we must distinguish the momentum growth associated with spreading within the primary resonance from diffusion that can occur after resonance overlap. This is accomplished by measuring the momentum transferred from a potential $V(x) = (\hbar\Omega_{\rm eff}/16)\cos(2k_L x)$ turned on and off as a square pulse with the same duration as the $\sin^2$ case. Here, there is only a single resonance which is identical to the primary resonance in the $\sin^2$ pulse due to the choice of relative amplitudes. Therefore, the rms prior to resonance overlap should be the same in both cases. After resonance overlap is crossed, there should be a distinct increase in the $\sin^2$ rms as compared with the square pulse. The experimental results in Fig. 3(a) show the rms momentum for both cases as a function of pulse duration

(rise and fall times of 25 ns are included in the square pulse duration). These agree well with classical numerical simulations in Fig. 3(b) and the estimated resonance overlap threshold. For the square pulse, the oscillation within the spatially periodic potential is clear and agrees with the single particle quantum description of the experimental atomic ensemble. Note that the crossing of the overlap threshold is clearly visible in the line shapes shown in Fig. 1 although the rms provides a simple quantitative signature.

In the limit of long pulse period one expects adiabatic behavior and in simple quantum systems such as the harmonic oscillator, the conditions for adiabaticity are clear. However, in nonlinear quantum systems there is generally not a single time scale, and the conditions for adiabaticity must be analyzed more carefully. A prominent feature in the phase portraits in Fig. 2 is the narrowing of the chaotic band, measured in momentum units of $2\hbar k_L$, with increasing pulse duration. This is seen easily by considering the width of the band of chaos given by $\Delta\rho/\bar{k}(= \Delta p/2\hbar k_L) = 2(1 + \sqrt{2k})/\bar{k}$ which on defining the pulse duration $T_s = \alpha\tau_{\rm HO}$ can be rewritten as

$$\frac{\Delta\rho}{\bar{k}} = \frac{\pi}{2\omega_r\tau_{\rm HO}} \frac{(1 + \alpha)}{\alpha}, \qquad (5)$$

Thus the number of states (separated by $2\hbar k_L$) within the chaotic band decreases with increasing pulse duration. A simple estimate for an adiabatic threshold is obtained by setting $\Delta\rho/\bar{k}$ equal to the initial thermal momentum spread of the atoms. Operationally, this condition requires the width of the chaotic band to be several times the width σ_p of the thermal Gaussian. For example, considering
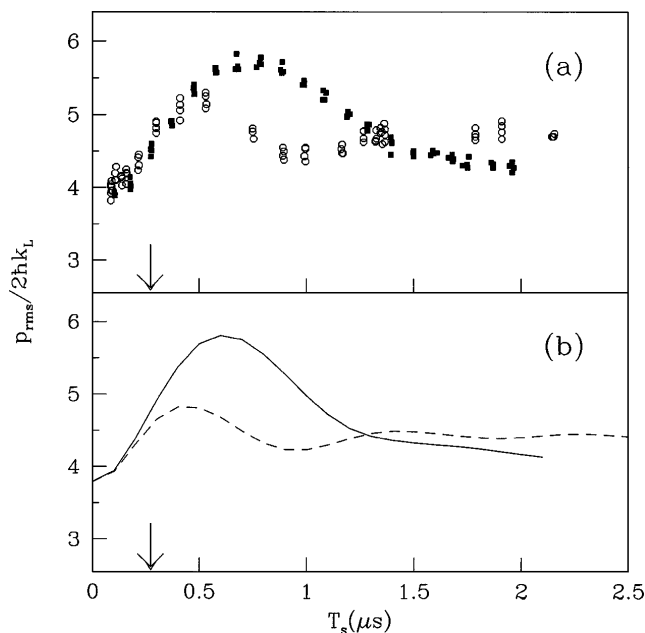
FIG. 3. (a) rms momentum computed from experimentally measured momentum distributions for $\sin^2$ (solid) and square (open) pulses. (b) The corresponding classical simulations are the solid and dashed lines. The threshold estimated from resonance overlap is indicated by the arrow. A clear deviation occurs at a pulse duration close to the predicted value. Note that an absolute power calibration was not available for these data, but the momentum transfer for the square pulse was consistent with $\Omega_{eff} = 41$ MHz. The initial momentum spread was 3.8 ± 0.2 in $2\hbar k_L$ units. For these parameter values, classical and quantum rms widths are in good agreement over the entire range of pulse times.

$\Delta\rho/\hbar = 4\sigma_p$ leads to

$$\alpha \geq \frac{1}{(8\sigma_p \omega_r/\pi)\tau_{HO} - 1}, \qquad (6)$$

which is valid when the denominator is positive and which shows a strong dependence on the initial momentum width. Thus, for the parameters of Fig. 2 ($\sigma_p = 2.9$) adiabatic behavior occurs only for times longer than ≈ 25 μs while for Fig. 3 ($\sigma_p = 3.8$) the threshold is ≈ 2 μs. These time scales are fully consistent with the experimental pulse durations where the line shape approaches the initial condition.

Our discussion has focused on the $\sin^2$ pulse profile, though these results can be applied to other pulse shapes. For example, earlier work on momentum transfer was performed in an atomic beam crossing a standing wave of light [10]. The resulting temporal pulse is then of the form $e^{-(t/T)^2}$. In practice, the laser beam profile has a natural cutoff imposed by spatial filtering which leads to a well-defined period of the pulse analogous to the pulse duration

in the $\sin^2$ profile. The potential can now be written as a discrete Fourier sum in multiples of this fundamental frequency and resonance overlap can result. Parameters where resonance overlap is significant can be attained though this was not the case for the parameters in Ref. [10].

In conclusion, we have tested experimentally the resonance overlap route to global classical chaos. These results illustrate that for nonlinear time dependent systems, novel physics can occur on intermediate time scales. This "gray zone" between fast passage and adiabatic interactions is, in fact, the generic situation and must be studied. In particular, interactions of standing waves of light with ultracold atoms clearly fall into this category and progress in control and manipulation of atomic motion must take these factors into account.

*Present address: NOAA/CMDL, Mail Stop R/E/CG1, Nitrous Oxide and Halocompounds Division, Boulder, CO 80303.

[1] A. L. Lichtenberg and M. A. Lieberman, *Regular and Chaotic Dynamics* (Springer-Verlag, Berlin, 1991).

[2] L. E. Reichl, *The Transition to Chaos in Conservative Classical Systems: Quantum Manifestations* (Springer-Verlag, Berlin, 1992).

[3] B. V. Chirikov, Phys. Rep. **52**, 265 (1979).

[4] G. H. Walker and J. Ford, Phys. Rev. **188**, 416 (1969).

[5] Resonance overlap in the stochastic heating of a plasma interacting with a large-amplitude standing wave was first reported by F. Doveil, Phys. Rev. Lett. **46**, 532 (1981). See A. Fasoli, F. Skiff, and M. Q. Tran, Phys. Plasmas **1**, 1452 (1994), for more recent results.

[6] R. Graham, M. Schlautmann, and P. Zoller, Phys. Rev. A **45**, R19 (1992).

[7] F. L. Moore, J. C. Robinson, C. Bharucha, P. E. Williams, and M. G. Raizen, Phys. Rev. Lett. **73**, 2974 (1994); J. C. Robinson, C. Bharucha, F. L. Moore, R. Jahnke, G. A. Georgakis, Q. Niu, M. G. Raizen, and Bala Sundaram, Phys. Rev. Lett. **74**, 3963 (1995). See also P. J. Bardroff, I. Bialynicki-Birula, D. S. Krähmer, G. Kurizki, E. Mayr, P. Stifter, and W. P. Schleich, Phys. Rev. Lett. **74**, 3959 (1995).

[8] Laser cooling and trapping is reviewed by Steven Chu in Science **253**, 861 (1991).

[9] F. L. Moore, J. C. Robinson, C. F. Bharucha, Bala Sundaram, and M. G. Raizen, Phys. Rev. Lett. **75**, 4598 (1995).

[10] See, for example, P. J. Martin, P. L. Gould, B. G. Oldaker, A. H. Miklich, and D. E. Pritchard, Phys. Rev. A **36**, 2495 (1987).